Solvation of Coumarin 480 within nano-confining environments: Structure and dynamics

M. Dolores Elola and Javier Rodriguez

Citation: The Journal of Chemical Physics **140**, 034702 (2014); doi: 10.1063/1.4861586
View online: http://dx.doi.org/10.1063/1.4861586
View Table of Contents: http://scitation.aip.org/content/aip/journal/jcp/140/3?ver=pdfcov
Published by the AIP Publishing

This article is copyrighted as indicated in the article. Reuse of AIP content is subject to the terms at: http://scitation.aip.org/termsconditions. Downloaded to IP: 168.96.66.131 On: Fri, 17 Jan 2014 17:04:27

Solvation of Coumarin 480 within nano-confining environments: Structure and dynamics

M. Dolores Elola[1,a)] and Javier Rodriguez[1,2]
[1]*Departamento de Física, Comisión Nacional de Energía Atómica, Avenida Libertador 8250, 1429 Buenos Aires, Argentina*
[2]*ECyT, UNSAM, Martín de Irigoyen 3100, 1650 San Martín, Provincia de Buenos Aires, Argentina*

(Received 9 October 2013; accepted 17 December 2013; published online 16 January 2014)

Equilibrium and dynamical characteristics pertaining to the solvation of the fluorescent probe Coumarin 480 within different confining environments are investigated using molecular dynamics simulations. Three kinds of confining systems are examined: (i) the cetyltrimethylammonium bromide (CTAB)/isooctane/1-hexanol/water; cationic inverse micelle (IM) (ii) a CTAB/water direct micelle (DM), and (iii) a silica-surfactant nanocomposite, comprising a cylindrical silica pore (SP) containing small amounts of water and CTAB species adsorbed at the pore walls. The solvation structures in the three environments differ at a qualitative level: an exchange between bulk- and interface-like solvation states was found in the IM, whereas in the DM, the solvation states of the probe are characterized by its embedding at the interface, trapped among the surfactant heads and tails. Within the SP structure, the coumarin exhibits alternations between internal and interfacial solvation states that occur on a ∼20 ns time scale and operate via 90° rotations of its molecular plane. The solvation responses of the environment following a vertical excitation of the probe are also investigated. Solvation times resulted between 2 and 1000 times longer than those found in bulk water, with a fast-to-slow trend IM→DM→SP, which can be interpreted in terms of the solvation structures that prevail in each case. © *2014 AIP Publishing LLC*. [http://dx.doi.org/10.1063/1.4861586]

I. INTRODUCTION

This study deals with the impact of confinement on the solvation of the fluorescent probe Coumarin 480 (C480) in three different media. This molecule represents a popular and versatile dye that has been used in previous experimental studies to examine solvation dynamics in a wide variety of polar and non-polar macroscopic liquid phases.[1–6] More recently, C480 has also been used to obtain information about the nature of the solvation in a series of inhomogeneous environments as well. Without being exhaustive, the list of systems investigated includes direct and inverse micelles,[7–10] lipid vesicles,[11] cyclodextrin cavities,[4,12] sol-gel matrices,[13] and silica-surfactant nanocavities,[14,15] to mention a few relevant examples.

The recent publication of three experimental studies focused on the solvation of C480 in confining environments sparked our interest of unveiling the microscopic characteristics of the structure and the dynamical mechanisms that control the solvation of this probe under these conditions. The first one corresponds to time-resolved experiments performed by Hazra *et al.*,[10] who have measured the solvation dynamics of water trapped within the cores of aqueous inverse micelles (IM), stabilized within an isooctane/1-hexanol organic phase by the surfactant cetyltrimethylammonium bromide (CTAB). Hazra *et al.*[10] reported average solvation times close to ∼7 ns, a value that clearly reveals the important retardations that take place in the overall dynamics of the confined aqueous phase, compared to the timescales observed in the isotropic bulk, which are in the picosecond time regime. Moreover, based on the fact that the observed retardations were roughly independent of the size of the water nano-pools, the authors concluded that the most stable solvation environment for the fluorescent probe seems to be the micellar interface. Similar conclusions were reported by Corbeil and Levinger in their experimental study on solvation dynamics in CTAB/1-pentanol/cyclohexane/water and CTAB/1-heptanol/cyclohexane/water IMs, using the anionic form of Coumarin 343 as a probe.[16]

Solvation dynamics of C480 in a related inhomogeneous environment, also combining CTAB and water, was examined in a second study by Sarkar *et al.*[7] At the experimental conditions investigated, the liquid phase includes nearly spherical, direct micelles of radius ∼3–4 nm, containing typically ∼80–100 surfactant molecules. The resulting structures of these moieties can be pictured in terms of a "dry" core, comprising the hydrocarbon tails, and an external, "wet," interface shell of thickness 6–9 Å, composed of the polar head groups and a sizeable fraction of the counterions as well. In these systems, the reported solvation times were found to be of the order of 0.5 ns, a temporal scale that is one order of magnitude shorter than that reported in IM with the same surfactant.

The third experimental study involved the analysis of the solvation of C480 within the interior of mesostructured silica-surfactant (CTAB) nanocomposites. We are referring to the work performed by Yamaguchi *et al.*[15] who employed time-resolved fluorescent techniques to analyze the characteristics of the solvation of coumarin dyes within cylindrical cavities

a)Electronic mail: DoloresElola@gmail.com

 © 2014 AIP Publishing LLC

This article is copyrighted as indicated in the article. Reuse of AIP content is subject to the terms at: http://scitation.aip.org/termsconditions. Downloaded to IP: 168.96.66.131 On: Fri, 17 Jan 2014 17:04:27

of silica-surfactant nanocomposites, built on a porous alumina membrane by surfactant-templated methods. In these cases, the resulting solvation times were found to exhibit a bi-modal character, with timescales of the order of ∼0.9 ns and ∼7.5 ns, respectively. Similar timescales were reported by Sahu *et al.*[14] who analyzed the solvation dynamics of C480 in a nanoporous sol-gel matrix in the presence of CTAB.

In an effort to provide a complementary description to this body of experimental information, in what follows, we will present results from massive molecular dynamics (MD) experiments on systems that closely reproduce the geometrical characteristics of the three different confining environments previously described. Our analysis will include not only structural characteristics pertaining to the solvation of the fluorescent probe but also information about particular features of its translational and orientational dynamics. In addition, we will also examine the solvation dynamics that follow a sudden change in the electronic distribution of the probe.

This paper is organized as follows: in Sec. II we describe the details of the model and the technical aspects of the simulation procedure. In Sec. III we analyze the main results of our study, in which we examine equilibrium and dynamical features of the probe within the different confining environments. Finally the concluding remarks are left for Sec. IV.

II. MODELS AND SIMULATION DETAILS

The systems under investigation were composed of a single coumarin C480 (see scheme on Fig. 1) embedded within three well differentiated confining environments: (i) an inverse aqueous micelle, i.e., a spherical-like water nano-pool stabilized within a non-polar phase by cationic surfactants; (ii) a direct micelle (DM) comprising a cationic surfactant moiety dissolved in water, and (iii) a water-saturated, silica pore of diameter ∼4 nm, with polar groups and surfactants adsorbed at the pore walls. All of them have in common the presence of CTAB as a surfactant species.

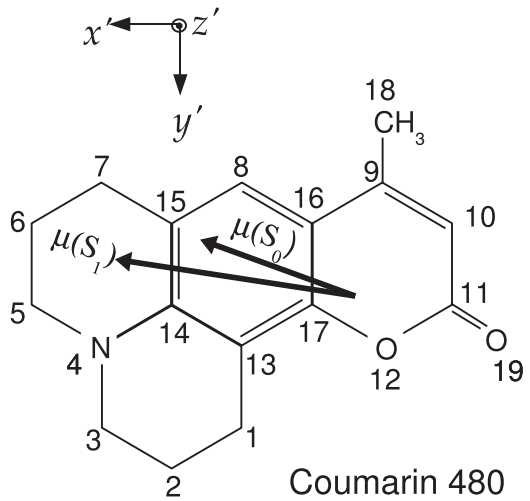

FIG. 1. Atom numbering used for Coumarin 480. The dipole moment vectors corresponding to the ground (S_0) and excited (S_1) states are also displayed on top of the molecule.

The different components were modeled as a collection of interaction sites. The potential energy of the system was considered as a sum of site-site, pair-decomposable contributions, and contains the usual terms from inter- and intramolecular interactions.

Water interactions were modeled by adopting the well-tested SPC/E potential.[17] On the other hand, the CTA^+ surfactant molecules were modeled as fully flexible units, including 62 interacting sites. Intra- and intermolecular interactions involving these sites were taken from the CHARMM27 force field.[18] In order to reduce computational costs, a simplified description for the mixed organic phase of the inverse micelle—combining isooctane and 1-hexanol—was implemented: methyl, methylene, CH, and OH groups were described via a united-atom model potential, taken from the GROMOS96 force field.[19] As such, each isooctane (hexanol) molecule involves a collection of 8 (7) sites. The inter- and intramolecular potential parameters employed for silica and silanol groups, were taken from Ref. 20. The fluorescent probe C480 was modeled as a fully flexible, ≈10 Å × 6 Å planar structure, comprising 36 interaction sites. The set of inter- and intramolecular parameters was taken from Ref. 21. The atomic partial charges of the probe were obtained according to the Merz-Singh-Kollman scheme.[22] The B3LYP/6-31G** level of calculation was employed for the description of C480 ground state, and for the case of its excited state, a superposition of singly excited Slater determinants (CIS/6-31G**) corresponding to ten different microstates was applied. All these computations were performed using the Gaussian03 software package.[23] This way of obtaining a reliable set of partial charges for the ground and excited states of the probe for MD simulations is a well-known and robust method, and it has been widely used by other groups in the past.[21,24–27] With this parametrization, the change in the dipolar moment between the ground and first excited states is $\Delta\mu = 3.6$ D. This value is in reasonable agreement with reported experimental values, obtained from time resolved microwave absorption techniques, which vary from $\Delta\mu = 3$ D up to 3.8 D.[28]

The preparation of the system involved a sequential procedure similar to that described previously in Refs. 29 and 30. The IM was constructed so as to reproduce experimental conditions[10] and consists of a 7 nm diameter, inner water pool surrounded by CTAB molecules, at a relative concentration of $w_0 = [H_2O]/[CTAB] = 23$ (see Table I). The external apolar phase includes an isooctane/1-hexanol, 9:1 v/v, mixture. The role of the explicit organic phase (along with a barostat setting to a P = 1 bar) is to essentially provide an equilibrating liquid-like environment for the reverse micelle,

TABLE I. Details of the simulations.

System	N_{CTAB}	N_w	R (Å)	ρ^{-1}_{CTAB} (Å^2)	Simul. box (Å^3)
(i) IM[a]	206	4752	35	56	150 × 150 × 150
(ii) DM	90	9160	25	87	70 × 70 × 70
(iii) SP	80	500	20	70	70 × 70 × 53

[a]The organic external phase contained $N_{iso} = 11566$ molecules of isooctane and $N_{hex} = 1684$ of 1-hexanol.

This article is copyrighted as indicated in the article. Reuse of AIP content is subject to the terms at: http://scitation.aip.org/termsconditions. Downloaded to IP: 168.96.66.131 On: Fri, 17 Jan 2014 17:04:27

allowing interface structural fluctuations in order to attain accurate densities inside the micelle. Moreover, these interface fluctuations would give rise to long wavelength collective dynamical modes that any realistic description of a reverse micelle in the nanosecond time scale should include. To build up the DM, the initial conditions were generated from a radial arrangement of 90 CTAB molecules conforming a spherical-like moiety of radius 25 Å (Ref. 31), surrounded by ∼9000 water molecules. Finally, we also build up a cylindrical silica pore of radius ∼20 Å, with silanol groups adsorbed at the pore walls with a surface density of $\rho_{SiOH} \sim 3\ nm^{-2}$, in agreement with experimental absorption data.[32] The interior of the pore was filled with adequate amounts of CTAB surfactants in a cylindrical arrangement. The overall orientation of the surfactants was such that their head groups remained in close contact with the pore walls, whereas the corresponding hydrophobic tails were located at the central part of the pore. The resulting area per surfactant group was ∼70 $Å^2$, which agrees reasonably well with the experimental conditions reported in Ref. 33. Along the full length of the simulation experiments, no meaningful modifications were observed in the overall surfactant structure inside the pore. Finally, water was allowed to permeate within the pore via a coupling with a "bulk" water reservoir, following the procedure described in detail in Refs. 34 and 35.

In all cases, the simulation protocol included initial equilibration periods of about 5 ns. In the simulation runs of micelles, this initial stage involved isobaric-isothermal runs whereas in the silica pore, due to the presence of a solid structure, the equilibration was performed along microcanonical trajectories. Meaningful statistics were collected along production runs, lasting typically 20–50 ns. All molecular dynamics trajectories were generated using the NAMD package.[36] Periodic boundary conditions were applied along the three Cartesian coordinates. Short-ranged intermolecular forces were cut off at 13 Å, while the particle mesh Ewald (PME) method was implemented to handle long-range Coulomb forces. The equations of motions were integrated using a multiple time step integration scheme, with a time step of 1 fs for intramolecular modes, 2 fs for non-bonded short-ranged forces, and 4 fs for the rest of the Coulomb forces. Additional details concerning Hamiltonian parameters and simulation procedures are provided in the supplementary material.[51] Table I displays the numbers of molecules and sizes of each simulated system. Figure 2 shows, schematically, the three systems, as well as some typical snapshots taken during the MD simulations.

Two kinds of simulation experiments were performed: (i) equilibrium averages of relevant observables related to the solvation of C480 in the ground state were collected along 20–50 ns, previously equilibrated, microcanonical trajectories; and (ii) non-equilibrium runs, in which the original charge distribution of C480 was switched, at $t = 0$, to that corresponding to the excited state. Initial conditions for these runs were taken from statistically independent configurations of the ground state trajectory, separated by 50 ps intervals. From these non-equilibrium initial configurations, the relaxations of the system were followed for about 30 ps in the case of micelles, and 200 ps in the case of the silica pore.

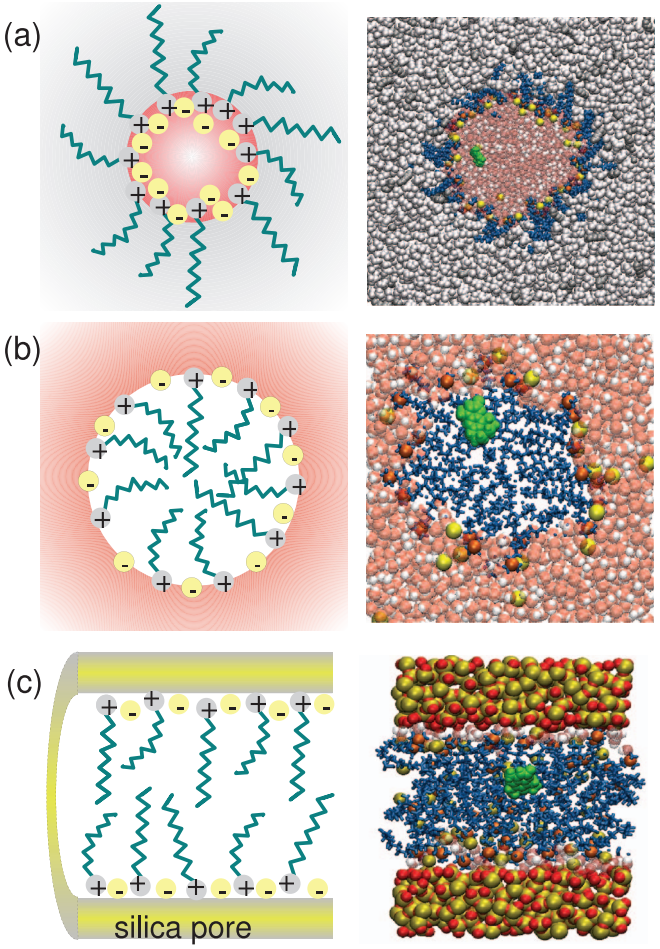

FIG. 2. Schemes of the three different confining systems in which the coumarin C480 was studied: (a) Inverse micelle CTAB/isooctane/1-hexanol/water; (b) direct CTAB micelle in water; and (c) cylindrical silica pore with CTAB and water. Typical snapshots captured during the MD simulations are shown on the right side.

III. RESULTS

A. Equilibrium local density profiles

We will start our analysis by examining local densities for a few relevant species along radial directions within the two different micelles investigated and the silica pore. The results correspond to ensemble averages collected along equilibrium trajectories, with the coumarin in its ground state. Assuming a spherical-like geometry for the micelle structures, a reasonable choice for the origin of a local reference system is their centers of mass. As such, density profiles for micellar systems were calculated as

$$\rho_\alpha(r) = \frac{1}{4\pi r^2} \sum_i \left\langle \delta\left(\left|\mathbf{r}_i^\alpha\right| - r\right)\right\rangle. \quad (1)$$

In the case of the cylindrical silica pore, the center of the local coordinate system was set at the center of mass of the solid block and the corresponding density profiles were computed from

$$\rho_\alpha(r) = \frac{1}{2\pi r L_z} \sum_i \left\langle \delta\left(R_i^\alpha - r\right)\right\rangle, \quad (2)$$

This article is copyrighted as indicated in the article. Reuse of AIP content is subject to the terms at: http://scitation.aip.org/termsconditions. Downloaded to IP: 168.96.66.131 On: Fri, 17 Jan 2014 17:04:27

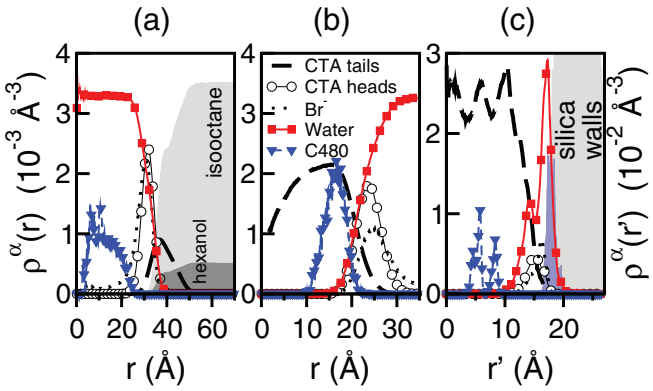

FIG. 3. Local density profiles of different species for the three systems investigated: (a) Inverse micelle CTAB/isooctane/1-hexanol/water; (b) direct CTAB micelle in water; and (c) silica nanopore with CTAB and water. The coumarin densities have been multiplied by a factor of 40 for better visualization; the water densities displayed in panels (a) and (b) are divided by a factor of 10. (Notice that the water bulk value at ambient conditions is $\rho^{wat} = 0.033$ Å^{-3}.) On panel (c), the dark-grey density peak corresponds to the hydrogen sites of SiOH groups at the internal surface of the pore; and the profile of CTA^+ tails is multiplied by 10 for better visualization.

where R_i^α denotes the distance between the position of site α in the ith molecule and the axis of the pore.

Results for the different $\rho_\alpha(r)$ are shown in Fig. 3. In the aqueous phase, we focused attention on the following species: water-oxygen, bromide ions, and the center of mass of the coumarin probe. Regarding the surfactant sites, we examined 4 atoms in the head groups (N and three C), whereas we also considered the set of 16 C atoms comprising the hydrophobic tails. Finally, for the organic phases, we considered the centers of mass of isooctane and 1-hexanol groups.

The structure of the inverse micelle CTAB/isooctane/1-hexanol/water is clearly characterized by three spatial domains (see Fig. 3(a)): on the one hand, an inner, $r \lesssim 20$ Å aqueous pool; on the other one, an external, $r \gtrsim 45$ Å region, where the organic species, isooctane and 1-hexanol, predominate. In between, one observes an intermediate third region, occupied by the bromide counterions and the CTA^+ surfactants, with their polar head groups in contact with the inner water pool and their hydrophobic tail groups lying at the most external region of the interface. Note that a major fraction of the Br^- ions (96%) remains associated with the cationic head groups, whereas the rest of free Br^- ions, are fully solvated by water, inside the micellar core. The density profiles corresponding to the surfactant head groups and the hydrophobic tails look both Gaussian-like, with widths of the order of ∼7 Å and 11 Å, respectively. Note that the coumarin probe explores the central region of the water pool, quite uniformly.

The density profiles corresponding to the direct CTAB micelle (Fig. 3(b)) also reveal three different regions: (i) a hydrophobic interior micellar core, composed exclusively of surfactant tail groups, which extends up to $r \sim 18$ Å; (ii) an external polar aqueous phase, beyond $r \sim 30$ Å; and (iii) an 18 Å $\lesssim r \lesssim$ 30 Å, intermediate Stern layer comprising the polar head groups, the bromide counterions, and a sizeable amount of water as well. Similarly to what we found in the inverse micelle case, a large fraction of the Br^- ions remains associated with the cationic head groups, at the most external side of the Stern layer, whereas a small fraction of the order of 15% remains solvated in the bulk-like aqueous phase. Contrasting, in this case, the coumarin remains located at the 10 Å $\lesssim r \lesssim$ 20 Å region, in contact with the hydrophobic tails.

The density profiles within the silica pores are plotted in Fig. 3(c). As a reference, the density profiles associated to Si and O atoms of the silica walls are represented as shaded regions. The presence of the surface polar Si–OH groups promotes a sensible increment of the local water density at the vicinity of pore walls: The profile exhibits a double-peaked structure which suggests at least two, tightly packed, layers. Note that the local density in the outmost one, is of similar order to the normal bulk value, $\rho^{wat}(r = 17$ Å$) \sim 0.03$ Å^{-3}. A more detailed analysis also shows that the latter layer remains hydrogen-bonded to the silanol groups at the interface, whereas the inner one, located ∼3 Å deeper into the pore would be in contact with the surfactant head groups. The bromide profile shows an intense external peak adjacent to the pore wall and a much milder internal shoulder, which would correspond to counterions bound to $[CTA]^+$ head groups. Finally, the inner portion of the pore is occupied by the surfactant tail groups, which exhibit a high degree of structure consisting of concentrical arrangement of layers, separated at regular 4–5 Å intervals, extending down to the center of the pore. Similarly to what we observed in the case of the direct micelle, the central hydrophobic region seems to provide the more stable environments for the solvation of the C480 probe. As a new element, the presence of some structure in the corresponding density profile would also suggest a manifold of stable solvation arrangements controlled by the intricacies of the local arrangement of the surfactant tails.

B. Translational and rotational dynamics

To gain a first insight into the dynamical characteristics of the probe within the confining environments, we will examine the time evolution of a few relevant parameters along equilibrium trajectories, with the probe in the S_0 state. In the three panels composing Fig. 4, we present time evolutions of $R(t)$, i.e., the distance between the center of mass of the probe and the micelle center (top and middle panels) and the pore axis (bottom panel). As a reference, we have included shaded regions that represent the locations of the surfactant head layers. At first glance, one observes clear differences in the magnitudes of the fluctuations of $R(t)$. Within the IM, in the course of a 20 ns time interval, the coumarin explores a wide range of radial distances, spanning from the micelle center up to $R(t) \sim 25$ Å. Moreover, exchange between bulk-like, i.e., inner solvation states, and interface ones was found to occur at intervals of, roughly, 1–4 ns. The time evolution of $R(t)$ within the direct micelle (middle panel) shows more restrictions in the radial displacements, since the probe remains mostly in contact with the inner boundary of the head group layer. More dramatic changes are observed in the silica pores (panel c) where the radial displacements of the probe are severely hampered. Note that, in this case, the translational dynamics of the probe can be pictured as a combination of fast, small

This article is copyrighted as indicated in the article. Reuse of AIP content is subject to the terms at: http://scitation.aip.org/termsconditions. Downloaded to IP: 168.96.66.131 On: Fri, 17 Jan 2014 17:04:27

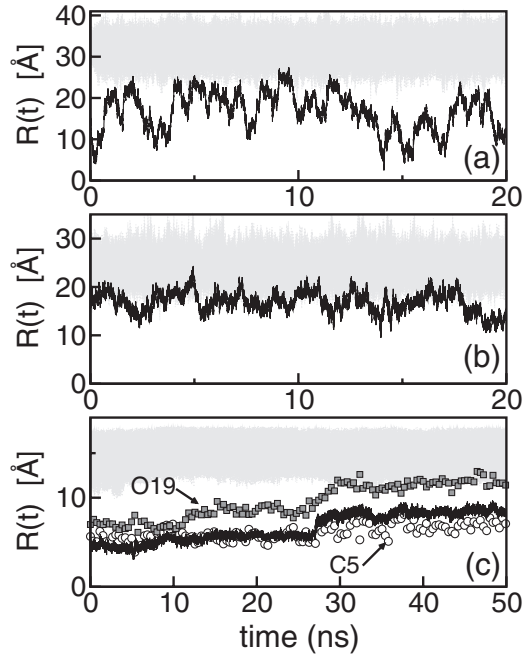

FIG. 4. Time evolution of the center-of-mass radial position of the coumarin, for the systems: (a) Inverse micelle; (b) direct micelle; and (c) silica pore. Note the expanded temporal scale on panel (c). The shaded regions represent the radial layer occupied by surfactant head groups. The radial distances to sites C5 (circles) and O19 (squares) of C480 are also plotted in panel (c).

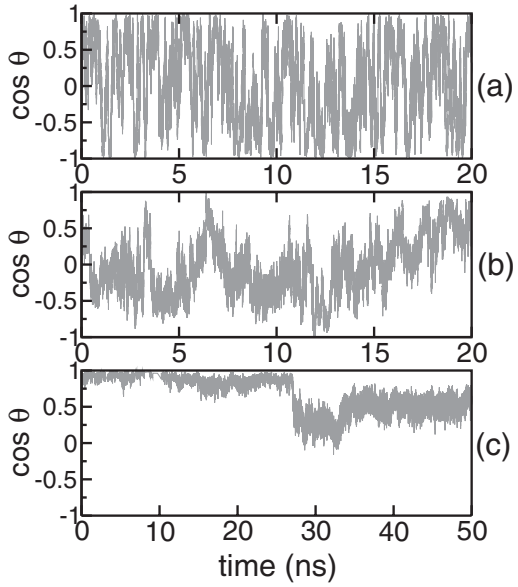

FIG. 5. Time evolution of the tilt angle $\cos\theta$ for the systems studied: (a) Inverse micelle; (b) direct micelle; and (c) silica pore. Note the longer scale for the x-axis on panel (c).

amplitude oscillations interrupted by sudden transitions, most notably the one clearly perceived at $t \sim 27$ ns. The additional discrimination of the radial distances involving the O19 and C5, distal groups reveals additional details of the probe dynamics. During the initial 10 ns, both radial distances look very much comparable (within 1–2 Å); an intermediate stage follows, in which the difference between these distances presents a moderate increment up to ∼ 3–4 Å before presenting a second abrupt jump, at $t \sim 27$ ns, after which they clearly differ by ∼6–7 Å.

To shed light into the latter feature, we found it convenient to also analyze the behaviors of orientational degrees of freedom. In Fig. 5 we present results for the time evolution for $\cos\theta(t)$, along the same trajectory analyzed previously. The latter variable represents the angle between the instantaneous radial coordinate of the C480 center of mass and a direction perpendicular to its molecular plane. Note that the characteristics of the three plots in Fig. 5 present features that seem to go hand-in-hand with those displayed in Fig. 4. In the inverse micelles, the probe exhibits full rotations along temporal intervals in the sub-nanosecond time domain whereas, in the direct micelles, the amplitude of orientational dynamics diminishes and the characteristic timescale stretches typically up to a few nanosecond. Interestingly, the three stages described in Fig. 4(c) are also clearly manifested in Fig. 5(c): during the initial 10 ns time interval, the probe remains solvated in the center of the pore, with its molecular plane practically perpendicular to the radial direction. The amplitude of the orientational fluctuations presents a twofold increment during the intermediate 10 ns $\lesssim t \lesssim$ 27 ns stage, as the probe approaches the head group layer. Finally, during the second half of the trajectory, rotational motions cease, as the probe remains with its molecular plane oriented in a $\theta \sim 75^\circ$, slanted geometry.

The previous observations can be gauged from a more quantitative perspective by analyzing time correlation functions (TCFs). In order to make contact with direct experimental information derived from time resolved fluorescent anisotropy measurements, we focused attention on single-dipole TCFs of the type

$$C_\mu^{(2)}(t) = \langle P_2[\cos\theta_\mu(t)]\rangle, \tag{3}$$

with

$$\cos\theta_\mu(t) = \frac{\boldsymbol{\mu}(0)\cdot\boldsymbol{\mu}(t)}{|\boldsymbol{\mu}^2|}. \tag{4}$$

In Eq. (3), $P_2(x) = (3x^2 - 1)/2$ is the second-rank Legendre polynomial, and $\boldsymbol{\mu}(t)$ in Eq. (4) represents the instantaneous transition dipole moment of the C480 which, in this case, was approximated by the μ_{S_0}.[37] Results for $C_\mu^{(2)}(t)$, for the different environments, are presented in Fig. 6 where, as a reference, we have also included results from simulations of C480 in bulk water. To extract dynamical information, the different functions $C_\mu^{(2)}(t)$ were fitted by bi- or tri-exponential functions of the type:

$$C_\mu^{(2)}(t) \approx \sum_{i=1}^{3} a_i \exp(-t/\tau_i). \tag{5}$$

Results for the different fitting parameters and for the overall rotational correlation times, $\tau_{\rm rot}$, extracted from time integrals of the single-dipole TCF,

$$\tau_{\rm rot} = \int_0^\infty C_\mu^{(2)}(t)\,{\rm d}t, \tag{6}$$

are listed in Table II. The analysis of the entries reveals that the orientational dynamics of the probe in bulk water and in inverse micelles are still comparable. Both decays can be

This article is copyrighted as indicated in the article. Reuse of AIP content is subject to the terms at: http://scitation.aip.org/termsconditions. Downloaded to IP: 168.96.66.131 On: Fri, 17 Jan 2014 17:04:27

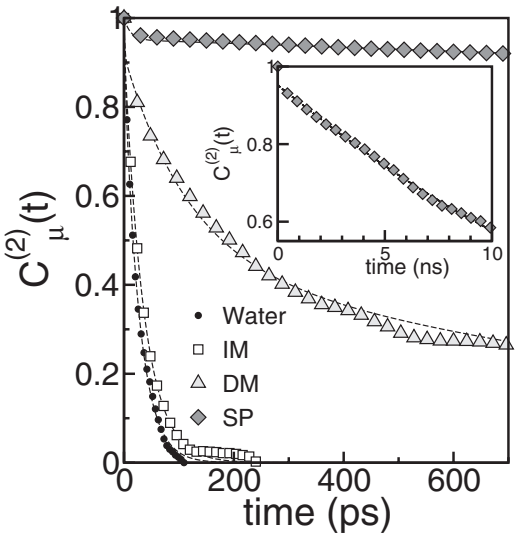

FIG. 6. Second-rank single dipole time correlation function of Coumarin 480 in the studied systems (with symbols). Solid lines represent the fitting functions. The inset shows the curve corresponding to the SP system, on a larger time scale of 10 ns.

reasonably well described by invoking two different timescales: the initial decorrelation is characterized by a fast $\tau_1 \sim 1$ ps; in addition, a second, somewhat slower, stage follows, characterized by τ_2 of the order of a few tens of picoseconds. For bulk water, our simulation experiments yield $\tau_{\rm rot} \sim$ 25 ps whereas for inverse micelles, the latter timescale was found to be 40% larger.

In the last column of Table II we have included results from time-resolved fluorescence anisotropy experiments. The direct comparison between the latter ones for bulk water and IM and our results reveals that, in both cases, our estimates fall too low compared to the experimental information. We can think of several possible reasons to account for such discrepancies: deficiencies in the parametrization of the adopted Hamiltonian are clearly one possibility. However, one should also keep in mind the inherent limitations in the temporal resolution of Hazra's setup, which are of the order of ∼80 ps. Note that Horng *et al.*[38] have also measured rotational dynamics of a similar coumarin (C153) in a series of solvents using a femtosecond up-conversion apparatus with much lower, 70 fs time resolution and reported typical values of $\tau_{\rm rot}$ in the order of 20–40 ps. Although neither the probe nor the solvent in Horng's experiments corresponds to the ones analyzed here, it is reasonable to infer that their results for $\tau_{\rm rot}$ should still be comparable to ours.

TABLE II. Fitting parameters for the second-rank single-dipole TCF of C480, $C^{(2)}_\mu(t) \approx \sum_{i=1}^{3} a_i \exp(-t/\tau_i)$, and rotational times ($\tau_{\rm rot}$) obtained by time integration of $C^{(2)}_\mu(t)$. Experimental data are also included, when available. Times are given in ps.

System	a_1	a_2	a_3	τ_1	τ_2	τ_3	$\tau_{\rm rot}$	$\tau^{\rm exp}_{\rm rot}$
Water	0.07	0.93	…	1.0	26.5	…	24.9	125[a]
								20–40 [b]
IM	0.05	0.95	…	1.0	35.5	…	33.7	281[c]
DM	0.08	0.46	0.46	1.5	115	1315	660	610[d]
SP	0.05	0.95	…	11.9	19600	…	(≳ 20 ns)	

[a]Reference 10.
[b]References 38 and 39.
[c]Reference 40.
[d]Reference 9.

Important retardations were registered for the orientational dynamics of C480 in direct CTAB micelles. In this case, the fitting procedure required a third exponential, with characteristic time of the order of 1 ns, a fact that stretched the overall temporal decay up to $\tau_{\rm rot} \sim 600$ ps. We remark that, in this case, our estimate agrees remarkably well with the one reported by Chakraborty *et al.*,[9] obtained from time-resolved experiments, which is listed in the last column of Table II.

Those dynamical modifications in the rotational dynamics of the probe are even more dramatic in silica pores. The plot in the inset of Fig. 6 shows that, after 10 ns, only half of the total orientational decorrelation has been achieved. These ultra-slow dynamical modes are exceedingly large to be accurately captured in the present simulations, so our characterization will be limited to this qualitative description. Still, given the structural similarities between the solvation scenarios prevailing in the decorated silica pore (SP) and the DM, one is led to believe that the large disparities between the corresponding values of $\tau_{\rm rot}$ could be somehow controlled by the differences in the rigidity of the confining framework. For the case of the DM, the persistence of large amplitude collective modes at the external interface could be transmitted to the interior of the moiety, benefiting the rotational dynamics of the probe. Contrasting, in the pore walls, the only remnant dynamical modes would be small amplitude vibrations which, in turn, would be insufficient to promote thermal fluctuations strong enough to lead to meaningful modifications in the orientation of the probe.

C. Solvation dynamics

The next aspect that we will investigate concerns the solvation dynamics of the probe. In time-resolved Stokes shift experiments,[41–43] the solvation response is usually reported in terms of the time evolution of $\nu(t)$, the frequency of the maximum of the fluorescence signal, via normalized response functions of the type:

$$S(t) = \frac{\nu(t) - \nu(\infty)}{\nu(0) - \nu(\infty)}. \tag{7}$$

In the previous equation, $\nu(\infty)$ corresponds to the maximum of the steady-state emission spectrum. Within the context of computer simulation studies, the latter function is equivalent to time-dependent relaxations of the solute-environment electrostatic energy gap, namely,[21,44,45]

$$S(t) = \frac{\langle \Delta E(t) - \Delta E(\infty) \rangle_{\rm ne}}{\langle \Delta E(0) - \Delta E(\infty) \rangle_{\rm ne}}, \tag{8}$$

where $\Delta E(t)$ represents the environment contribution (i.e., water, surfactant, counterions, and pore walls) to the energy gap between the S_1 and S_0 Born-Oppenheimer potential energy surfaces of the probe at time t:[21,44]

$$\Delta E(t) = \sum_{\alpha \in \rm C480} \Delta q_\alpha \, V_\alpha(t). \tag{9}$$

This article is copyrighted as indicated in the article. Reuse of AIP content is subject to the terms at: http://scitation.aip.org/termsconditions. Downloaded to IP: 168.96.66.131 On: Fri, 17 Jan 2014 17:04:27

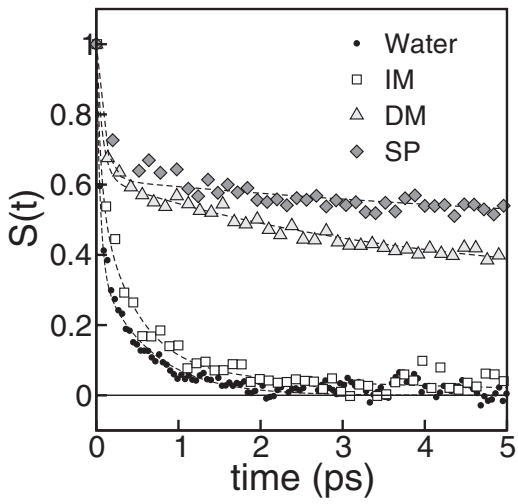

FIG. 7. Short-time solvation response function $S(t)$, for Coumarin 480 in different environments, obtained from 500 nonequilibrium independent trajectories for each system. Dashed lines represent the fitting functions.

In the previous equation, Δq_α and $V_\alpha(t)$ represent the charge jump and the electrostatic potential at the solute site α, respectively:

$$V_\alpha(t) = \sum_{j \notin \mathrm{C480}} \frac{q_j}{r_{\alpha j}(t)}. \tag{10}$$

In Eq. (10), the label j refers to all charged sites in the system, other than those of the probe. Angular brackets of the type $\langle \cdots \rangle_{\mathrm{ne}}$ in Eq. (8) denote an average obtained from a set of non-equilibrium trajectories.

In Fig. 7 we present results for $S(t)$. The values of $\Delta E(\infty)$ in Eq. (8) were estimated from $\langle \Delta E \rangle_{\mathrm{eq}}^{\mathrm{S_1}}$, i.e., the equilibrium ensemble averages of the energy gaps collected along a 20 ns equilibrium trajectory with the coumarin in its first excited state S_1.

Quantitative estimates of solvation characteristic times can be inferred from time integrals of $S(t)$, namely,

$$\tau_{\mathrm{slv}} = \int_0^\infty S(t)\mathrm{d}t. \tag{11}$$

Results for τ_{slv} are listed in Table III, along with the best fitting parameters.

The direct inspection of Fig. 7 reveals that the set of solvation responses exhibits two well differentiated characteristics: on the one side, the responses of pure water and inverse micelles present decays that practically vanish after ~1 ps. The characteristics of these relaxations have been described in previous studies in terms of initial, inertial decays—involving time scales in the sub-picosecond time domain—operated via librational motions of the water molecules. Diffusive, slower tails are also observed, with characteristic timescales of the order of a few picoseconds. The entries in the two upper rows in Table III corroborate the previous description although, in IM case, we found it necessary to include a third slower timescale $\tau_3 = 4.3$ ps that could be ascribed to a non-negligible extent of dynamical heterogeneity from water molecules in the IM, in close contact with the surfactant species. Contrasting, after ~1 ps, solvation processes in DM and in silica pores are half-way towards their full relaxations and both exhibit temporal decays characterized by values of τ_3 which are, at least, between one and two orders of magnitude larger than those found in the previous two cases (bulk water and IM).

TABLE III. Solvation fitting parameters, $S(t) \approx \sum_{i=1}^{3} a_i \exp(-t/\tau_i)$, and solvation times ($\tau_{\mathrm{slv}}$) obtained by time integration of $S(t)$. Experimental and convoluted solvation times are also listed when available (see text). Times are given in ps.

System	a_1	a_2	a_3	τ_1	τ_2	τ_3	τ_{slv}	$\tau_{\mathrm{slv}}^{\mathrm{exp}}$	$\tau_{\mathrm{slv}}^{\mathrm{conv}}$
Water	0.64	0.36	…	0.05	0.63	…	0.26	0.23[a]	…
IM	0.43	0.50	0.07	0.06	0.50	4.3	0.56	7000[b]	…
DM	0.38	0.28	0.34	0.07	3.4	115	40	474[c]	435
SP	0.38	0.18	0.44	0.06	7.8	660	292	4000[d]	1360

[a]Reference 4.
[b]Reference 10.
[c]Reference 7.
[d]Reference 15.

The expression in Eq. (10) shows that the solvation response includes contributions from all the different charged species surrounding the probe. These contributions, in principle, may exhibit different dynamical characteristics. So, it is useful to decompose the full response into its different contributions, S_i, namely,

$$S(t) = \sum_i c_i\, S_i(t), \tag{12}$$

with

$$c_i = \frac{\langle \Delta E_i(0) - \Delta E_i(\infty) \rangle_{\mathrm{ne}}}{\langle \Delta E(0) - \Delta E(\infty) \rangle_{\mathrm{ne}}} \tag{13}$$

and

$$S_i(t) = \frac{\langle \Delta E_i(t) - \Delta E_i(\infty) \rangle_{\mathrm{ne}}}{\langle \Delta E_i(0) - \Delta E_i(\infty) \rangle_{\mathrm{ne}}}. \tag{14}$$

In the previous equations, c_i represents the fractional contribution of the ith component ($i = \mathrm{CTA^+}$, $\mathrm{Br^-}$, water or eventually SiOH species) to the Stokes shift, while $S_i(t)$ is the normalized solvation response of component i to the charge jump operated in the C480 solute. The relative weights of the different species to the total energy gap are displayed in Table IV, along with our estimates for the total Stokes shifts, $\Delta\nu = \langle \Delta E(0) - \Delta E(\infty) \rangle$, and the corresponding experimental values.

TABLE IV. Solvation parameters for the solvation of C480 confined within different environments.

System	c_{CTA}	c_{Br}	c_{w}	$\Delta\nu$ ($\mathrm{cm^{-1}}$)	$\Delta\nu^{\mathrm{exp}}$
IM	0.066	0.024	0.910	1256	1410[a]
DM	0.286	0.004	0.710	914	490[b]
SP	0.306	0.131	0.507	599	510[c]
Water				1553	1340[d]

[a]Reference 10.
[b]Reference 7.
[c]Reference 15.
[d]Reference 4.

This article is copyrighted as indicated in the article. Reuse of AIP content is subject to the terms at: http://scitation.aip.org/termsconditions. Downloaded to IP: 168.96.66.131 On: Fri, 17 Jan 2014 17:04:27

A few important comments concerning this set of data are in order: (i) Note that the values $\Delta\nu$ exhibit a gradual reduction in passing from the most polar (bulk water) towards the much less polar environment (in our case, the silica pore). Despite the variety of systems and different experimental techniques implemented, one can conclude that the overall agreement with the experimental results is acceptable, with the exception of the DM entry, for which our result is a factor of ∼2 higher than the value reported in Ref 7. (ii) The modifications in the overall polarity promote a gradual reduction in the water contribution and a concomitant increment in the surfactant response (expressed in terms of c_w and c_{CTA}, respectively). Still, in the three confined environments, the major contribution to the decay of the energy gap comes from the water molecules. The latter observation is somehow unexpected, considering that, for example, in the case of SP, the water content in close contact with the probe barely exceeds, typically, ∼1–2 molecules. A detailed analysis of water and surfactant contributions to the total Stokes shift, by integrating contributions of molecules lying within a sphere of radius d centered at the coumarin center-of-mass, showed that the few water molecules that lie within a sphere of radius $d \sim 7$ Å around the C480, already accounts for 85% of the total aqueous contribution. A closer inspection of the structure near the probe revealed that the closest water molecules around the C480 are those acting as hydrogen bond (HB) donors to the O12 and O19 sites of the coumarin. A rough estimate of the difference in the energy gaps associated with the small changes in O19-water distances upon excitation yields a Stokes shift of $\Delta\nu \sim 210$ cm^{-1}. In a related context, Ramegowda[46] investigated, in a recent work, by electronic structure calculations, the coumarin 1-$(H_2O)_3$ complex in vacuum. The author analyzed the contribution of the nearest hydrogen bonded water molecules to the relaxation of the excited state of the dye, and found that a minimal variation (less than 0.1 Å) in the distance between one or two water molecules H-bonded to the carbonyl moiety of the coumarin could yield a decrease of about 5–6 kJ/mol (≈500 cm^{-1}) in the energy gap between excited and ground states of the complex.

The overall picture that would emerge from this more detailed analysis suggests that the retardations operated in the overall solvation response not only do they reflect modifications in the diffusive and orientational behaviors of the water molecules as a result of the restrictions in their mobilities, but also an increment of contributions from inherently more massive—and consequently slower—groups which lie in the vicinity of the probe. The plots in Fig. 8 provide helpful information to gauge the real differences between the dynamical characteristics of the solvation responses from the two major contributors, i.e., S_w and S_{CTA}, in the more sluggish environments. Note that the confinement brings the water response practically comparable to the CTA^+ one, a fact that would reveal a high degree of coupling between the dynamical modes of these two species operated by the characteristics of the prevailing confinement.

Before closing this section, we would like to bring into consideration a final aspect related to the comparison between the present simulation results and the experimental

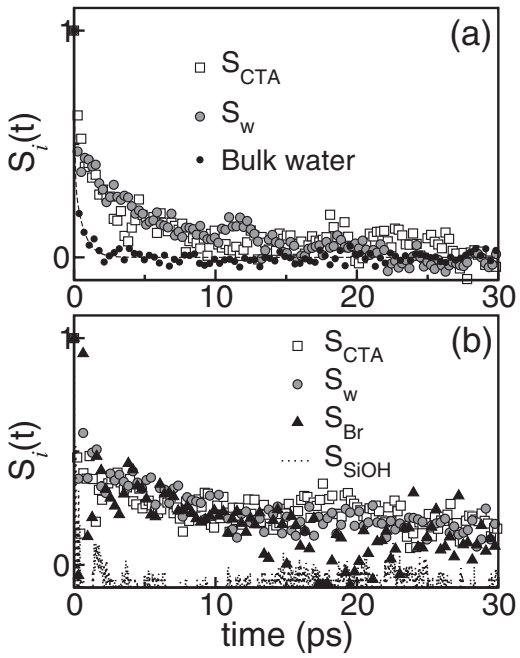

FIG. 8. Normalized contributions from different species, $S_i(t)$, to the total solvation response of C480 trapped in a direct micelle (a) and in a silica nanopore (b).

ones, listed in columns 8 and 9 of Table III. As we mentioned in Sec. III B, such comparison is not straightforward and, in fact, the two sets of results should be considered as complementary pieces of information: on the one hand, the temporal resolutions of the experimental setups are, normally, not enough to capture ultrafast components of the solvation whereas, on the other hand, and due to the wide interval of relevant time scales—which span over practically 6 orders of magnitude—the simulations are not sufficiently long to harvest reliable statistics for dynamical processes characterized by timescales beyond a few nanoseconds. As expected, the more sluggish the particular dynamical response considered, the more marked the disparities observed. In a related context, also note, for example, that the temporal resolution reported in Ref. 15 for SPs is of the order of 200 ps. Under these circumstances, additional technical problems should also be considered, such as those related to the finite fluorescence lifetime of the probe, which may affect the ability to accurately capture the complete decay of $S(t)$ or, even, the actual magnitude of $\Delta\nu$.

From the simulation perspective, a crude modification, which takes into account effects from temporal resolutions, can be easily incorporated by convoluting the solvation response with a Gaussian-like window function, yielding shifted responses of the type:[47]

$$S^{\text{conv}}(t) = \frac{1}{\sqrt{2\pi}\,\Delta}\int_0^{2t_0} \frac{S(t'+t)}{S(t_0)}\,\exp\left[-\frac{(t'-t_0)^2}{2\Delta^2}\right]\mathrm{d}t', \tag{15}$$

where t_0 is the time shift related to the temporal resolution of the experiments whereas the width Δ should be chosen much smaller than t_0. In Fig. 9 we present plots for the original non-equilibrium relaxations $S(t)$ and their convoluted counterparts $S^{\text{conv}}(t)$, whereas in the last column of Table III we report

This article is copyrighted as indicated in the article. Reuse of AIP content is subject to the terms at: http://scitation.aip.org/termsconditions. Downloaded to IP: 168.96.66.131 On: Fri, 17 Jan 2014 17:04:27

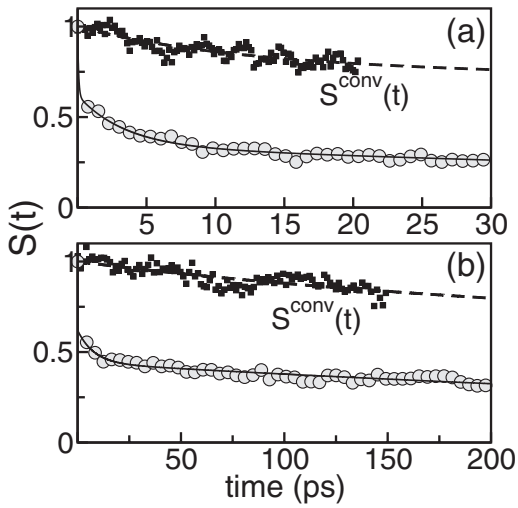

FIG. 9. Comparison between the computed solvation response before [$S(t)$, circles] and after convolution with a Gaussian function representing the instrument time resolution [$S^{conv}(t)$ with squares, Eq. (15)], for (a) the direct micelle and (b) the silica pore cavity. Symbols correspond to the computed responses and lines, to the fitting functions. The Gaussian is centered at $t_0 = 10$ ps for the DM and at $t_0 = 50$ ps in the SP.

values of τ_{slv}^{conv}, the time integrals of $S^{conv}(t)$ computed by setting $t_0 = 10$ ps and $t_0 = 50$ ps for DM and SP, respectively ($\Delta = 50$ fs in both cases). Note that the latter values are comparable to the reported temporal resolutions of the experimental setups and bring simulation and experimental results in a much more reasonable agreement.

Finally, we would like to refer to a recent work performed by Guchhait and Biswas,[48] in which they investigate AOT/water reverse micelles of different sizes, with a trapped Coumarin 153, by MD simulations and dynamic fluorescence techniques. Their MD simulation results suggest that the solute resides always close to the interface, and the average relaxation times of rotation and solvation of the probe are of the order of hundreds of picoseconds, substantially longer than those observed in bulk water. Important differences appear when both MD simulations are contrasted: (i) The use of different approaches for modeling the reverse micelles. In the work of Guchhait and Biswas the interior of the reverse micelle was approximated as a rigid spherical cavity and the external organic phase was not included. Consequently, the long wavelength collective dynamical modes at the interface were not explicitly considered in their model. (ii) The consideration of different surfactants (CTAB versus AOT) may have major consequences on the overall dynamics. Recent results obtained by infrared spectroscopy[49] showed that when the anionic AOT surfactant is changed by a chemically different surfactant, the cationic CTAB, the dynamical features of the micelle are markedly different. (iii) The use of different probes—C480 in this work and C153 in Guchhait's one. The fact that both probes are structurally comparable does not necessarily imply that they behave in the same way, even when they are confined in a similar environment. Indeed, Rao *et al.*[50] analyzed the dynamic relaxation of C153 and C480 in direct micelles and found a probe dependent solvation dynamics that they assign to different locations of those molecules within the micelles. As a consequence, we believe that the comparison between the results obtained from both MD simulations is far to be straightforward. Reverse micelles are complex systems in which the presence of charged species, irregular interfaces, and highly inhomogeneous density distributions may preclude any attempt of generalization; special caution should be exerted when general conclusions are drawn from a given particular case.

IV. CONCLUDING REMARKS

We have presented molecular dynamics simulation results that provide microscopic structural details and dynamical information about the solvation of Coumarin 480 in three different environments, in which CTAB acts as a cationic surfactant. Two of them correspond to soft confining structures involving an inverse micelle of radius 35 Å and a direct one of radius close to 30 Å. The third system corresponds to a water filled, rigid cylindrical silica pore of radius 20 Å, with hydrophilic OH-terminated walls, containing CTAB surfactants.

Concerning the spatial localization of the coumarin in inverse micelles, our simulation results reveal the presence of solvation states mainly at the center of the aqueous pool, in which the rotational dynamics of the probe is ∼33% slower than the one in aqueous bulk phases. On the other hand, in direct micelles, the probe localizes mainly at the interface region, embedded among the tail groups of the CTAB surfactant, a fact that brings the rotational dynamics even slower, with a characteristic solvation time which is approximately 25 times longer than the one observed in the bulk. In the cylindrical silica pore, water exhibits a two-layer structure at the vicinity of the silica walls: (i) the outer one, highly-packed and hydrogen-bonded to the surface silanol groups, and (ii) a more internal second one, located ≈3 Å inward, solvating the surfactant head groups and counterions. Moreover, the location of the coumarin presents alternations between internal and interfacial solvation states, controlled by 90° rotations of the coumarin plane, which require characteristic time spans of the order of ∼20 ns, to be fully achieved.

We followed the relaxations of the solvent energy gap upon the vertical excitation ($S_0 \rightarrow S_1$) of the probe, along non-equilibrium trajectories for about 30 ps in the IM and DM cases, and along 200 ps in the SP one. The characteristic solvation times were found to be between 2 and 1000 times longer than those normally recorded in isotropic phases of water, with a fast-to-slow trend similar to the one registered for the rotational dynamics, previously described.

A decomposition analysis of the total solvation response reveals that water molecules still provide the main contributions to the solvation decay in IM and DM systems—90% and 70%, respectively—in spite of the remarkable reduction in the average number of water molecules that lye in the closest shell solvation of the probe. This feature still persists in SP, in which one observes a 50% water contribution despite an even more drastic (≈95%) drop of the water content in the first solvation shell.

The comparison between MD simulation results and experimental time-resolved data is also presented. The direct comparison between computed solvation times and those reported in direct experiments exhibits large disparities that can

This article is copyrighted as indicated in the article. Reuse of AIP content is subject to the terms at: http://scitation.aip.org/termsconditions. Downloaded to IP: 168.96.66.131 On: Fri, 17 Jan 2014 17:04:27

be systematically reduced by convoluting the computed responses with a Gaussian window-like functions that take into account limitations in the temporal resolution of the experimental techniques.

ACKNOWLEDGMENTS

We are grateful to Daniel Laria for many fruitful discussions and valuable suggestions regarding this manuscript. J.R. thanks financial support from ANPCyT (Grant No. PICT2007-00300) and M.D.E. thanks financial support from CONICET (Grant No. PIP112-2008-00403). M.D.E. and J.R. are staff members of CONICET, Argentina.

[1]R. W. Yip, Y. X. Wen, and A. G. Szabo, J. Phys. Chem. **97**, 10458–10462 (1993).
[2]R. S. Moog, D. L. Bankert, and M. Maroncelli, J. Phys. Chem. **97**, 1496–1501 (1993).
[3]N. P. Wells, M. J. McGrath, J. I. Siepmann, D. F. Underwood, and D. A. Blank, J. Phys. Chem. A **112**, 2511–2514 (2008).
[4]S. Vajda, R. Jimenez, S. J. Rosenthal, V. Fidler, G. R. Fleming, and E. W. Castner, J. Chem. Soc., Faraday Trans. **91**, 867 (1995).
[5]D. Chakrabarty, P. Hazra, A. Chakraborty, D. Seth, and N. Sarkar, Chem. Phys. Lett. **381**, 697–704 (2003).
[6]P. K. Mandal, A. Paul, and A. Samanta, Res. Chem. Intermediates **31**, 575–583 (2005).
[7]N. Sarkar, A. Datta, S. Das, and K. Bhattacharyya, J. Phys. Chem. **100**, 15483 (1996).
[8]N. Sarkar, K. Das, A. Datta, S. Das, and K. Bhattacharyya, J. Phys. Chem. **100**, 10523 (1996).
[9]A. Chakraborty, D. Chakrabarty, P. Hazra, D. Seth, and N. Sarkar, Chem. Phys. Lett. **382**, 508 (2003).
[10]P. Hazra, D. Chakrabarty, A. Chakraborty, and N. Sarkar, Chem. Phys. Lett. **382**, 71 (2003).
[11]P. Sen, T. Satoh, K. Bhattacharyya, and K. Tominaga, Chem. Phys. Lett. **411**, 339 (2005).
[12]A. Douhal, Chem. Rev. **104**, 1955–1976 (2004).
[13]S. K. Pal, D. Sukul, D. Mandal, S. Sen, and K. Bhattacharyya, J. Phys. Chem. B **104**, 2613 (2000).
[14]K. Sahu, D. Roy, S. K. Mondal, A. Halder, and K. Bhattacharyya, J. Phys. Chem. B **108**, 11971 (2004).
[15]A. Yamaguchi, Y. Amino, K. Shima, S. Suzuki, T. Yamashita, and N. Teramae, J. Phys. Chem. B **110**, 3910 (2006).
[16]E. M. Corbeil and N. E. Levinger, Langmuir **19**, 7264–7270 (2003).
[17]H. J. C. Berendsen, J. R. Grigera, and T. P. Straatsma, J. Phys. Chem. **91**, 6269 (1987).
[18]A. D. MacKerell, Jr., N. Banavali, and N. Foloppe, Biopolymers **56**, 257 (2000).
[19]L. D. Schuler, X. Daura, and W. F. van Gunsteren, J. Comput. Chem. **22**, 1205 (2001).
[20]J. Rodriguez, M. D. Elola, and D. Laria, J. Phys. Chem. B **114**, 7900 (2010).
[21]P. V. Kumar and M. Maroncelli, J. Chem. Phys. **103**, 3038 (1995).
[22]U. C. Singh and P. A. Kollman, J. Comput. Chem. **5**, 129–145 (1984).
[23]M. J. Frisch, G. W. Trucks, H. B. Schlegel *et al.*, GAUSSIAN 03, Revision C.02, Gaussian, Inc., Pittsburgh, PA, 2003.
[24]S. J. Rosenthal, R. Jimenez, G. R. Fleming, P. V. Kumar, and M. Maroncelli, J. Mol. Liq. **60**, 25 (1994).
[25]F. Cichos, R. Brown, U. Rempel, and C. von Borczyskowski, J. Phys. Chem. A **103**, 2506–2512 (1999).
[26]L. R. Martins and M. S. Skaf, Chem. Phys. Lett. **370**, 683 (2003).
[27]F. Ingrosso, B. M. Ladanyi, B. Mennucci, and G. Scalmani, J. Phys. Chem. B **110**, 4953 (2006).
[28]A. Samanta and R. W. Fessenden, J. Phys. Chem. A **104**, 8577 (2000).
[29]J. Rodriguez, J. Martí, E. Guàrdia, and D. Laria, J. Phys. Chem. B **111**, 4432 (2007).
[30]M. H. H. Pomata, D. Laria, M. S. Skaf, and M. D. Elola, J. Chem. Phys. **129**, 244503 (2008).
[31]T. Imae, R. Kamiya, and S. Ikeda, J. Colloid Interface Sci. **108**, 215–225 (1985).
[32]T. Kamijo, A. Yamaguchi, S. Suzuki, N. Teramae, T. Itoh, and T. Ikeda, J. Phys. Chem. A **112**, 11535 (2008).
[33]G. D. Stucky, A. Monnier, F. Schüth, Q. Huo, D. Magolese, D. Kumar, M. Krishnamurty, P. Petroff, A. Firouzi, M. Janicke, and B. F. Chmelka, Mol. Cryst. Liq. Cryst. **240**, 187–200 (1994).
[34]M. D. Elola, J. Rodriguez, and D. Laria, J. Chem. Phys. **133**, 154707 (2010).
[35]M. D. Elola, J. Rodriguez, and D. Laria, J. Phys. Chem. B **115**, 12859 (2011).
[36]J. C. Phillips, R. Braun, W. Wang, J. Gumbart, E. Tajkhorshid, E. Villa, C. Chipot, R. D. Skeel, L. Kale, and K. Schulten, J. Comput. Chem. **26**, 1781 (2005).
[37]The orientational fluctuations were measured with respect to the dipole moment in the S_0 state. This description should be equivalent to the one provided by the transition dipole moment.
[38]M. L. Horng, J. A. Gardecki, and M. Maroncelli, J. Phys. Chem. A **101**, 1030 (1997).
[39]T. Pradhan, P. Ghoshal, and R. Biswas, J. Chem. Sci. **120**, 275–287 (2008).
[40]P. Hazra, D. Chakrabarty, and N. Sarkar, Chem. Phys. Lett. **371**, 553–562 (2003).
[41]M. Maroncelli, J. Mol. Liq. **57**, 1 (1993).
[42]P. F. Barbara and W. Jarzeba, "Ultrafast photochemical intramolecular charge and excited state solvation," in *Advances in Photochemistry* (John Wiley & Sons, Inc., Hoboken, NJ, 2007), Vol. 15.
[43]E. W. Castner, Jr., and M. Maroncelli, J. Mol. Liq. **77**, 1 (1998).
[44]M. Maroncelli and G. R. Fleming, J. Chem. Phys. **89**, 5044 (1988).
[45]M. Maroncelli, J. Chem. Phys. **94**, 2084 (1991).
[46]M. Ramegowda, Res. J. Chem. Sci. **3**(7), 25–30 (2013).
[47]L. R. Martins, A. Tamashiro, D. Laria, and M. S. Skaf, J. Chem. Phys. **118**, 5955 (2003).
[48]B. Guchhait, R. Biswas, and P. K. Ghorai, J. Phys. Chem. B **117**, 3345–3361 (2013).
[49]A. M. Dokter, W. Sander, and H. J. Bakker, J. Chem. Phys. **126**, 124507 (2007).
[50]V. G. Rao, C. Banerjee, S. Mandal, S. Ghosh, and N. Sarkar, Spectrochim. Acta A **102**, 371–378 (2013).
[51]See supplementary material at http://dx.doi.org/10.1063/1.4861586 for additional details regarding the preparation of the simulated systems, and a list of the atomic partial charge parameters of C480.

This article is copyrighted as indicated in the article. Reuse of AIP content is subject to the terms at: http://scitation.aip.org/termsconditions. Downloaded to IP: 168.96.66.131 On: Fri, 17 Jan 2014 17:04:27